Inflammation Research (2022) 71:1095–1108
https://doi.org/10.1007/s00011-022-01605-y

Inflammation Research

ORIGINAL RESEARCH ARTICLE

Heme oxygenase-1 protects against endotoxin-induced acute lung injury depends on NAD^+-mediated mitonuclear communication through PGC1α/PPARγ signaling pathway

Simeng He[1] · Jia Shi[1] · Wenming Liu[1] · Shihan Du[1] · Yuan Zhang[1] · Lirong Gong[1] · Shuan Dong[1] · Xiangyun Li[1] · Qiaoying Gao[2] · Jing Yang[2] · Jianbo Yu[1]

Received: 26 April 2022 / Accepted: 28 June 2022 / Published online: 11 July 2022

Abstract

Endotoxin-induced acute lung injury (ALI) is a challenging life-threatening disease for which no specific therapy exists. Mitochondrial dysfunction is corroborated as hallmarks in sepsis which commonly disrupt mitochondria-centered cellular communication networks, especially mitonuclear crosstalk, where the ubiquitous cofactor nicotinamide adenine dinucleotide (NAD^+) is essential for mitonuclear communication. Heme oxygenase-1 (HO-1) is critical for maintaining mitochondrial dynamic equilibrium and regulating endoplasmic reticulum (ER) and Golgi stress to alleviating acute lung injury. However, it is unclear whether HO-1 regulates NAD^+-mediated mitonuclear communication to exert the endogenous protection during endotoxin-induced ALI. In this study, we observed HO-1 attenuated endotoxin-induced ALI by regulated NAD^+ levels and NAD^+ affected the mitonuclear communication, including mitonuclear protein imbalance and UPR^{mt} to alleviate lung damage. We also found the protective effect of HO-1 depended on NAD^+ and NAD^+-mediated mitonuclear communication. Furtherly, the inhibition of the PGC1α/PPARγ signaling exacerbates the septic lung injury by reducing NAD^+ levels and repressing the mitonuclear protein imbalance and UPR^{mt}. Altogether, our study certified that HO-1 ameliorated endotoxin-induced acute lung injury by regulating NAD^+ and NAD^+-mediated mitonuclear communications through PGC1α/PPARγ pathway. The present study provided complementary evidence for the cytoprotective effect of HO-1 as a potential target for preventing and attenuating of endotoxin-induced ALI.

Keywords Heme oxygenase-1 · NAD^+ · Acute lung injury · Mitonuclear communication · Sepsis

Introduction

Sepsis, a systemic inflammatory response to infection, is characterized by a life-threatening organ dysfunction [1]. Pulmonary is one of the most susceptible target organs in response to sepsis, with a mortality rate as high as 35–46% [2, 3]. Since the worldwide pandemic of coronavirus disease 2019 (COVID-19), approximately 15% presented with severe pneumonia and 5% of patients eventually progress to acute respiratory distress syndrome (ARDS), septic shock, and/or multiple organ dysfunction [4, 5]. Therefore, exploring specific strategies to prevent and treat acute lung injury (ALI) or ARDS remains urgently needed.

Mitochondrial dysfunction contributes to a hallmark of and a driving force behind endotoxin-related ALI and primarily as a source of metabolic and oxidative stress [6–9]. As a center of energy-harvesting and intermediate metabolism of cells, mitochondria have developed complex communication networks with other cellular components, such as endoplasmic reticulum (ER), lysosomes, and cytosolic pathways, which actively influence metabolic and signaling activities [9, 10]. Of note, the well-characterized crosstalk for mitochondrial stress has cooperated with the nucleus,

Simeng He, Jia Shi and Wenming Liu contributed equally to this work.

✉ Jianbo Yu
30717008@nankai.edu.cn

[1] Department of Anesthesiology and Critical Care Medicine, Tianjin Nankai Hospital, Tianjin Medical University, Tianjin, China

[2] Tianjin Key Laboratory of Acute Abdomen Disease Associated Organ Injury and ITCWM Repair, Institute of Acute Abdominal Diseases of Integrated Traditional Chinese and Western Medicine, Tianjin Nankai Hospital, Tianjin, China

known as mitonuclear communication which represents adaptive processes, including mitonuclear protein imbalance and the mitochondrial unfolded protein response (UPR^{mt}) [11–17]. Accumulating evidence suggested that mitonuclear communication conferred protective properties to mitigating mitochondrial dysfunction deriving from oxidative stress [15, 18, 19]; thus, strategies that preserve mitonuclear communication in septic settings are essential for reserving cellular homeostasis and might be a potential therapeutic target.

Heme oxygenase-1 (HO-1), a stress-inducible protein together with heme-related catabolic products carbon monoxide (CO) and bilirubin, is closely related to mitochondrial respiratory function and oxidative phosphorylation, which are crucial for counteracting inflammation or oxidative stress [7, 20–22]. Under stress conditions, HO-1 performs endogenous protective effects against endotoxic end-organ damage by its anti-inflammatory, anti-apoptotic, and antioxidant properties [7]. We have previously confirmed that the HO-1/carbon monoxide system is integral to mitochondrial dynamic equilibrium by modulating the balance of mitochondrial fusion and fission to alleviate ALI [21, 23–25]. Besides, HO-1 attenuates lung damage by regulating ER stress and Golgi stress, but proof of mitonuclear communication is still lacking [25, 26].

Nicotinamide adenine dinucleotide (NAD^+) is a vital cofactor for multiple metabolic reactions, which is essential for maintaining mitonuclear communication [10, 27–29]. Increasing lines of evidence have demonstrated that NAD^+ are pivotal contributors to sensing and communicating the mitochondrial metabolic status to other cellular compartments to safeguard cellular and organismal fitness [10, 11]. Approaches target enhancing the NAD^+ concentrations are beneficial for inhibiting oxidative stress and alleviating the acute lung damage [30–32]. However, whether the protective effect of NAD^+ alleviates lung injury by regulating mitonuclear communication is poorly understood. Intriguingly, HO-1 and its metabolite CO are intimately linked to NAD^+ metabolism [33]. Therefore, we speculated that the lung-protective effect of HO-1 might be related to the regulation of NAD^+. The current study was designed to elucidate whether NAD^+ alleviated endotoxin-induced ALI by preserving mitonuclear communication, and then studies were to explore whether the protective effect of HO-1 depends on NAD^+-mediated mitonuclear communication and the underlying molecular mechanism.

Materials and methods

Animals

Wild-type C57BL/6 J mice (aged 6–8 weeks, weighting 20–22 g, Male) were supplied by the Laboratory Animal Center of Tianjin Nankai Hospital (Tianjin, China). Well-characterized HO-1 conditional-knockout mice ($HO\text{-}1^{fl/fl}CAG^{CreERT2}$, $HO\text{-}1^{-/-}$) and NMNAT1 conditional-knockout mice ($NMNAT1^{flox}R26^{CreERT2}$, $NMNAT1^{-/-}$) on a C57BL/6 J background were generated by Beijing Biocytogen Co., Ltd. The HO-1 gene was induced by tamoxifen (Sigma, USA), which was specifically performed as our previous studies [23, 25], and the NMNAT1 gene was induced by tamoxifen dissolved in corn oil at a concentration of 10 mg/ml, which injected intraperitoneally once a day for a total of five consecutive days and waited for one week. All the mice were maintained at 25 °C with 12 h light and dark photocycle, and they have free access to food and water ad libitum throughout the study period. All animal experiments were performed in accordance with the legislation on laboratory animals and approved by the Animal Care and Use Committee of the Tianjin Nankai Hospital (Approval No. NKYY-DWLL-2019-012, Tianjin, China).

Experimental protocols

To evaluate the effect of HO-1 on endotoxin-induced ALI, wild-type (WT) and $HO\text{-}1^{-/-}$ mice were divided into five groups ($n = 6$): WT, WT + LPS, WT + LPS + Hemin, $HO\text{-}1^{-/-}$, and $HO\text{-}1^{-/-}$ + LPS. Animals were anesthetized with 2–3% isoflurane (R510-22, RWD Life Science) for induction and 1–1.5% isoflurane for maintenance. LPS (*E.coli*-L2630, Sigma, USA) 15 mg/kg diluted in 2 ml saline was injected via caudal vein for wild-type and $HO\text{-}1^{-/-}$ mice as previously described [23]. And the mice in WT + LPS + Hemin group were pretreated with 30 mg/kg hemin (Sigma, USA) intraperitoneally 2 h prior to LPS administration. To explore the effect of NAD^+ on LPS-induced ALI, wild-type and $NMNAT1^{-/-}$ mice were assigned to five groups ($n = 6$): WT, WT + LPS, $NMNAT1^{-/-}$, $NMNAT1^{-/-}$ + LPS, and $NMNAT1^{-/-}$ + LPS + NMN. Of note, NMN (500 mg/kg, Sigma, USA) was injected intraperitoneally 1 h before LPS injection. To determine whether the effect of HO-1 depends on NAD^+ and PGC1α/PPARγ pathway, wild-type and $NMNAT1^{-/-}$ mice were divided into WT + LPS + Hemin, $NMNAT1^{-/-}$ + LPS + Hemin, and WT + LPS + Hemin + SR-18292, 45 mg/kg SR-18292 (Med Chem Express, USA) was intraperitoneally injected into mice 1 h prior to LPS treatment. Additionally, an equal volume of DMSO or sterile saline was used as a control vehicle.

After LPS attacked for 12 h, the mice were euthanized with efforts were made to minimize animals' suffering. Blood samples were drawn from the retro-orbital vein of isoflurane-anesthetized mice and centrifuged at 3000*g* for 10 min at 4 °C for serum analysis. In addition, the lung tissues were harvested for histological assessment or stored at − 80 °C for further biochemical analysis.

Histopathological evaluation

The formaldehyde-perfused middle lobe of the right lung was fixed, sectioned, and routinely stained with hematoxylin and eosin. The histopathology of the lung injury was scored quantitatively as described previously [7, 34]. The injury score was based on the following characteristics: alveolar septa, hemorrhage, intra-alveolar fibrin, and leukocyte infiltration from ten different fields by light microscopy (×200). Each characteristic was scored (0: normal to 4: very severe) by a pathologist blinded to the experiment.

Lung W/D ratio

The wet-to-dry weight (W/D) ratio was measured to the degree of pulmonary edema. After weighing the wet weight (W), tissues were desiccated at 65 °C for 48 h to obtain the dry weight (D).

Assessment of myeloperoxidase (MPO) activity

MPO activity from lung tissue was measured by an MPO detection kit (A044-1-1, Nanjing Jiancheng, China) following the instructions. In short, lung tissues were homogenized and the supernatant was subjected to reaction buffer in a water bath at 60 °C for 10 min; then the OD 460 nm was evaluated by a spectrophotometer (Lambda 35, PerkinElmer, USA). The activities of MPO are presented in U/g tissue.

Transmission electron microscopy

The lung tissues were fixed in 2.5% glutaraldehyde in 0.1 M phosphate buffer (pH 7.4) for 2 h at room temperature. Then specimens were post-fixed with 1% osmium tetroxide for 3 h, dehydrated in a gradient series of ethanol, embedded in acetone, and sectioned approximately at 70 nm. Ultrathin sections were cut with the Leica Ultracut E ultramicrotome (Leica, Germany), then stained with 3% uranyl acetate and lead citrate. Finally, the ultrastructure was viewed using the JEM-1230 transmission electron microscope (JEOL Instrument, Japan) which operated at an acceleration voltage of 80 kV.

Detection of mitochondrial membrane potential (ΔΨm)

Changes in ΔΨm were evaluated by fluorescent dyes 5,5′,6,6′-tetrachloro-1,1′,3,3′-tetraethylbenzimidazolcarbocyanine iodide (JC-1) assay kit (Beyotime, China), according to the manufacturer's instructions as described before [35]. The isolated mitochondria (2 mg/ml) were stained with JC-1 (310 nmol/L) in the darkness at 37 °C for 30 min, washed twice in cold JC-1 staining buffer, and then incubated with a normal medium. The fluorescence intensity in the mitochondria was indicated by a fluorescence emission (Em) wavelength shift from green (530 nm) to red (590 nm) following excitation (Ex) at 488 nm, while JC-1 monomer in the cytosol transferred to the mitochondrial matrix cumulatively. The ratio of J-aggregate^{+}-mitochondria (red) and JC1^{+}-mitochondria (green) was used to assess ΔΨm using the flow cytometer (EXFLOW 206, Dakewe, China).

Detection of mitochondrial ROS

A Mitochondria isolation kit (Thermo Scientific) was used for mitochondria fraction preparation, as previously reported [23]. Mitochondrial ROS was measured by using 2',7'-dichlorofluorescein diacetate (DCFH-DA) probe (Solarbio, China) for 30 min at room temperature, then washed three times with PBS, and collected in a glass slide containing PBS. The fluorescence signal was measured respectively at excitation and emission wavelength of 488 nm and 520 nm by a microplate reader. The fluorescent images were assessed using Image pro-Plus software and the results for WT group were expressed as a relative reference.

Detection of NAD^{+} and NAD^{+}/NADH ratio

Determination of NAD^{+} and NADH concentrations was evaluated using NAD^{+}/NADH assay kits (Abbkine, China) according to the manufacturer's protocols. The detection of NAD^{+} and NADH was based on a glucose dehydrogenase cycling reaction, in which tetrazolium dye 3-(4,5-dimethyl-2-thiazolyl)-2,5-diphenyltetrazolium bromide (MTT) was reduced by NADH in the presence of phenazine methosulfate. Briefly, 61 µL assay buffer, 12 µL MTT, 1 µL NAD cycling enzyme mix, and 1 µL PES were mixed as working reagent, adding 40 µL sample and 80 µL working reagent per well. Then, the 565 nm OD values were used to determine NAD^{+} and NADH concentration from the standard curve.

Reverse transcription-quantitative polymerase chain reaction

Total RNA was isolated from lung tissues using the DNeasy Blood and Tissue kits (Qiagen, Germany) and was converted into cDNA using Prime-Script RT reagent Kit (Takara, Japan). All PCR products were amplified using the following thermocycling conditions: 95 °C for 10 min, followed by 40 cycles of 95 °C for 15 s and 60 °C for 1 min (ABI-7500 Sequence Detection System, Applied Biosystems, USA). Additionally, the $2^{-\Delta\Delta Ct}$ method was used to quantify the gene expression, and values were reported as an average of triplicate analyses. Primer sequences are listed in Table 1.

Table 1 Primer for qRT-PCR

Genes	Forward sequence (5′–3′)	Reverse sequence (5′–3′)
GAPDH	CCTGGAGAAACCTGCCAAGTA	GGAAGAGTGGGAGTTGCTGTTG
TNF-α	GGCAGGTCTACTTTGGAGTCATTGC	ACATTCGAGGCTCCAGTGAATTCGG
IL-6	CCACTGCCTTCCCTACTTCA	TCTTGGTCCTTAGCCACTCC
IL-1β	GCTGCTTCCAAACCTTTGAC	AGCTTCTCCACAGCCACAAT
mtDNA fragment	CCCAGCTACTACCATCATTCAAGT	GATGGTTTGGGAGATTGGTTGATG
nDNA internal	GCCAGCCTGACCCATAGCCATAATAT	AGAGATTTTATGGGTGTAATGCGG

Measurement of mitochondrial DNA copy number (mtDNA-CN)

Mitochondrial DNA copy number (mtDNA-CN) is related to mitochondrial enzyme activity and biosynthesis and can therefore serve as a hallmark of mitochondrial function. Total DNA was extracted using the DNeasy Blood and Tissue kits (Qiagen, Germany), and mtDNA-CN was determined and analyzed as described previously [23]. The mtDNA-CN was evaluated by the ratio of mtDNA to nuclear DNA (nDNA) using quantitative polymerase chain reaction (qPCR). The specific primes of mtDNA are shown in Table1.

Western blot analysis

The proteins from right lung tissues were extracted using a total protein isolation kit (Solarbio, China), the concentrations of protein were quantified by the BCA protein assay kit (Solarbio, China), and 30 μg of protein was loaded per well on 10% SDS-PAGE for electrophoresis. Subsequently, proteins were transferred to PVDF membranes (Bio-Rad, USA) and blocked with 5% skimmed milk in TBST for 3 h at room temperature. Then, membranes were incubated at 4 °C overnight with primary antibodies for HO-1 (1:1000, CST5061S), MTCO1(1:2000, ab14705), SDHA (1:2000, ab14715), HSP60 (1:1000, ab190828), LONP1 (1:1000, ab224316), HSP90 (1:2000, ab13492), PPARγ (1:1000, ab178860), PGC1α (1:2000, ab106814), and β-actin (1:3000, AF7018). After washing five times with TBST, the membranes were incubated with appropriate horseradish peroxidase-conjugated secondary antibody (1:3000, S0001) for 1 h at room temperature. Proteins were visualized by an enhanced chemiluminescence Western blot detection kit (170-5070, Bio-Rad, USA). The relative expression of target proteins was quantified by the ImageJ-Analysis system, and β-actin served as a standard reference.

Statistical analysis

All experiments were performed at least thrice with similar results and data are expressed as mean ± SD. Paired t-test was used for comparisons between two groups and one-way analysis of variance (ANOVA) was conducted followed by Bonferroni post hoc test for comparisons among groups. Statistical analyses were performed using GraphPad Prism 8.3.0 (GraphPad Software Inc.). P value of < 0.05 was considered significant ($^{*}P < 0.05$, $^{**}P < 0.01$).

Results

HO-1 alleviated the pulmonary pathologic damage and increased NAD^+ levels

HO-1 is a stress-inducible protein that mediates antioxidant and anti-inflammatory effects and maintains cellular homeostasis under stress conditions [23, 36]. To observe the effect of HO-1 on endotoxin-induced ALI, we performed identical experiments using WT and $HO^{-/-}$ mice subjected to LPS administration. As expected, an obvious decrease in HO-1 mRNA and protein level was found in $HO\text{-}1^{-/-}$ mice relative to wild-type mice under the same conditions. LPS stimulation surged an adaptive upregulation of HO-1, and the precursor Hemin pretreatment increased HO-1 expression significantly (Fig. 1A and B), which is consistent with our previous observation [7]. As illustrated in Fig. 1D, LPS administration induced typical pathological characteristics, including alveolar hemorrhage, thickened alveolar septa, infiltrated inflammatory cells, and accompanied by an increased lung injury score (Fig. 1C and D). Hemin pretreatment remarkably mitigated the pulmonary injury and decreased the scores (Fig. 1C and D). However, the pathologic changes were more extensive and severe in $HO\text{-}1^{-/-}$ mice subjected to LPS than WT mice, and the semiquantitative score of lung damage was elevated consistently (Fig. 1C and D).

Furthermore, the pro-inflammatory factors, W/D ratio, and MPO activity were detected to reflect the pulmonary inflammation and the degree of lung edema. Compared with controls, septic mice showed a noticeable higher W/D ratio, MPO activity, and cytokines, including IL-1β, TNF-α, and IL-6, while hemin suppressed pulmonary edema, neutrophil recruitment, and release of inflammatory factors (Fig. 1E–G). $HO\text{-}1^{-/-}$ mice subjected to LPS exhibited

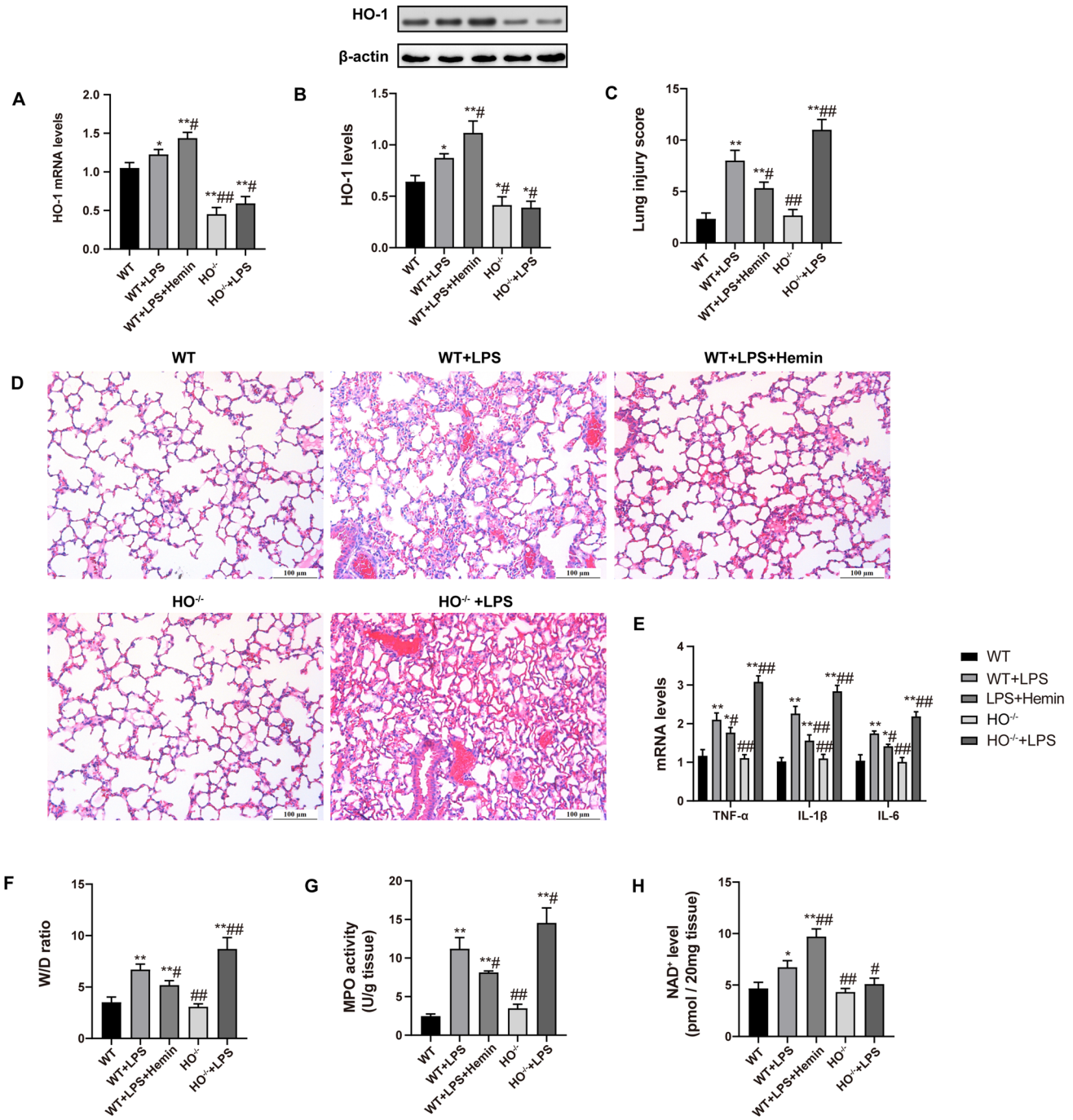

Fig. 1 HO-1 attenuated the septic lung injury and increased NAD^+ levels. **A** Expressions of the mRNA levels of HO-1. **B** Representative bands and quantification of HO-1. **C** Semiquantitative evaluation of ALI using lung injury scores. The grading scale of 0 = minimal damage, 1 + = mild damage (25%), 2 + = moderate damage (50%), 3 + = severe damage (75%), and 4 + = maximal damage (almost 100%). **D** The image of histopathologic changes of lung tissue with H&E staining (×200). **E** Expressions of the mRNA levels of pro-inflammatory cytokines TNF-α, IL-1β, and IL-6. **F** The W/D ratio. **G** MPO activity. **H** The contents of NAD^+ were determined with an NAD^+/NADH Assay Kit. Values are expressed as mean ± SD and were analyzed by one-way ANOVA corrected with Bonferroni coefficient. $^{*}P<0.05$, $^{**}P<0.01$ versus WT group and $^{\#}P<0.05$, $^{\#\#}P<0.01$ versus WT + LPS group, respectively

marked inflammatory exudation and edema relative to WT mice (Fig. 1E–G). Collectively, these indicators supported a key role for HO-1 in attenuating septic lung injury.

To investigate whether the protective effect of HO-1 might be involved in NAD^+, the sensors, and guardians of homeostasis, we next examined the levels of NAD^+. As

shown in Fig. 1H, NAD^+ levels exerted defensive increases for WT mice subjected to LPS relative to controls, and hemin pretreatment ahead of LPS stimulation induced a distinct increase in NAD^+ contents (Fig. 1H). However, compared with the WT + LPS group, NAD^+ levels were dramatically decreased in HO-$1^{-/-}$ mice exposed to LPS (Fig. 1H). Therefore, the relationship between the lung-protective effect of HO-1 and NAD^+ levels was highly correlated.

NAD^+ deficiency aggravated septic lung injury, whereas NAD^+ supplementation ameliorated the injury

Substantial evidence has accumulated that NAD^+ homeostasis plays a crucial role in host–pathogen interactions which is important in regulating oxidatice stress [30, 37]. NMNAT1 has been identified as the highest catalytic activity in NAD^+ biosynthesis, and NMN supplementation can increase NAD^+ availability via the NAD^+ salvage pathway in mice [38, 39] (Fig. 2A), thus knockout NMNAT1 conditional and exogenous NMN supplementation intraperitoneally can modulate NAD^+ concentrations and then observe the altered NAD^+ on ALI. NAD^+ levels were significantly decreased in NMNAT$1^{-/-}$ mice, while NMN supplementation led to an apparent elevation of NAD^+ (Fig. 2B). However, LPS caused an adaptive increase in NAD^+ levels in wild-type mice and a similar upregulation in NMNAT$1^{-/-}$ mice (Fig. 2B).

To further investigate the effect of NAD^+ on LPS-induced acute lung injury of mice, pro-inflammatory cytokine levels and lung histopathology were evaluated. As shown in

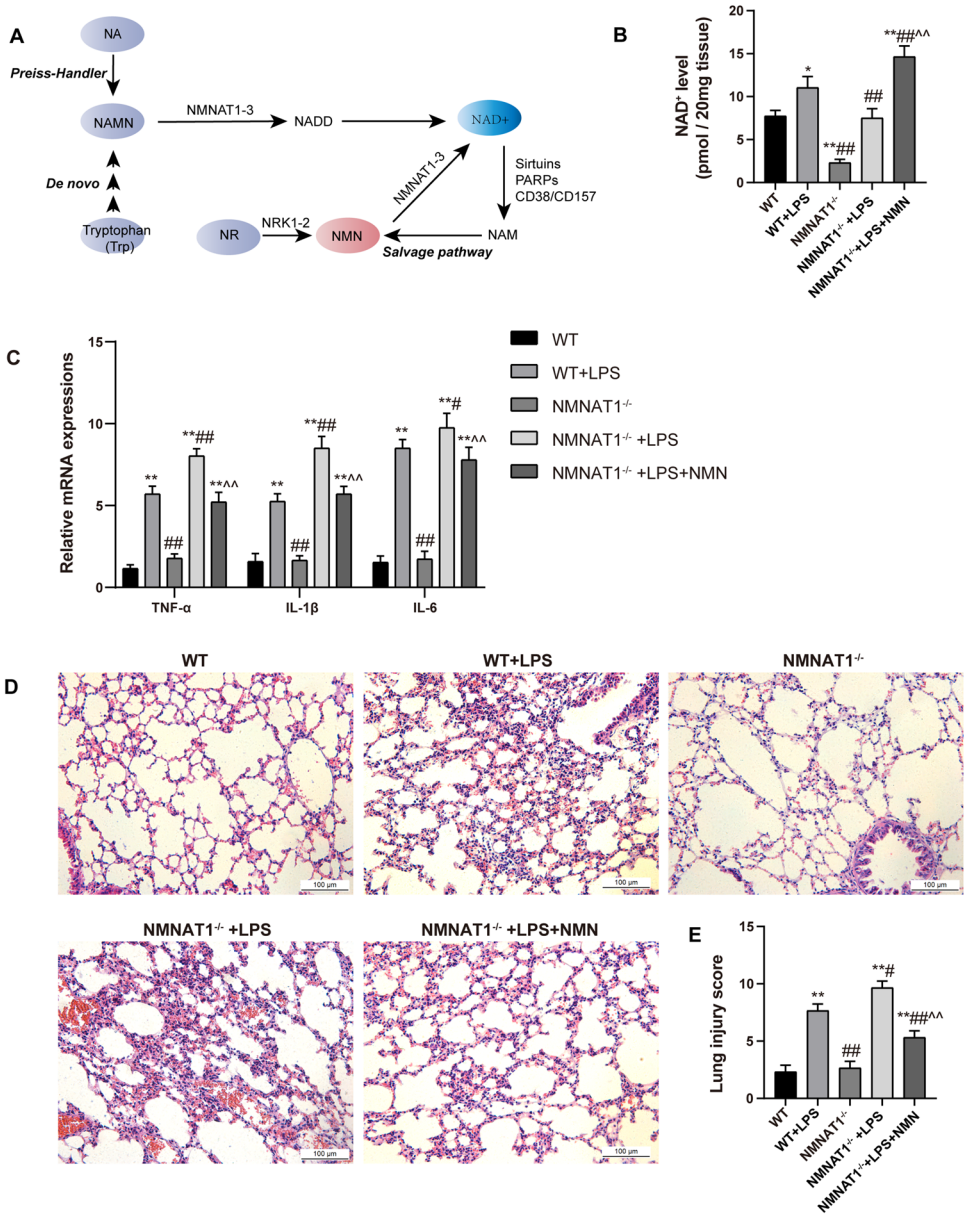

Fig. 2 Effect of NAD^+ levels on sepsis-related ALI. **A** Schematic of the NAD^+ biosynthetic pathway. **B** NAD^+ contents in lung tissue. **C** Relative mRNA levels of inflammatory cytokines TNF-α, IL-1β, and IL-6 were determined. **D** Representative hematoxylin/eosin (H&E) staining of lung sections (×200). **E** Semiquantification of pathological scores according to the pathological observation. Data are presented as mean ± SD and group comparisons were analyzed by one-way ANOVA followed by Bonferroni post hoc test. $^{*}P<0.05$, $^{**}P<0.01$ versus WT group, $^{\#}P<0.05$, $^{\#\#}P<0.01$ versus WT + LPS group, and $^{\wedge}P<0.05$, $^{\wedge\wedge}P<0.01$ versus NMNAT$1^{-/-}$ + LPS group, respectively

Fig. 2C, exposure to LPS both in WT and NMNAT1$^{-/-}$ mice showed a striking increase in levels of TNF-α, IL-β, and IL-6, which were significantly suppressed by pretreatment with NMN. Besides, the pro-inflammatory factor mRNA levels markedly increased in NMNAT1$^{-/-}$ mice subjected to LPS relative to WT mice (Fig. 2C). The photomicrographs of lung slices revealed that NMNAT1$^{-/-}$ mice exhibited thinner alveolar septa, even some malnourished but without typical lesions relative to WT mice, which might attribute to the central role of NAD$^+$ in energy metabolism (Fig. 2D). Compared with the WT + LPS group, cellular infiltration, edema, fibrin exudation, and neutrophil recruitment were severe in the NMNAT1$^{-/-}$ + LPS group, whereas restoring NAD$^+$ contents with exogenous NMN supplementation attenuated the lung injury (Fig. 2D). Additionally, the semiquantitative assessment showed that lung injury scores in NMNAT1$^{-/-}$ mice received LPS were higher than those in WT mice, while decreased in NMN treatment (Fig. 2E). Together, these results validated the critical role of NAD$^+$ in sepsis-induced ALI that its deficiency aggravated the lung damage, while NAD$^+$ supplementation attenuated the injury.

NAD$^+$ protected against mitochondrial oxidative damage and preserved morphology in mice challenged by LPS

The imbalance of ROS production led to a burst of oxidative stress, further mtDNA damage, and loss of mitochondrial membrane potential (ΔΨm), which resulted in an abnormal mitochondrial ultrastructure [40]. There were striking increases in mitochondrial ROS and mtDNA but a decline of ΔΨm with the altered architecture of mitochondria in WT + LPS group relative to controls (Fig. 3A–E). Remarkably, NMNAT1$^{-/-}$ mice that received LPS displayed more

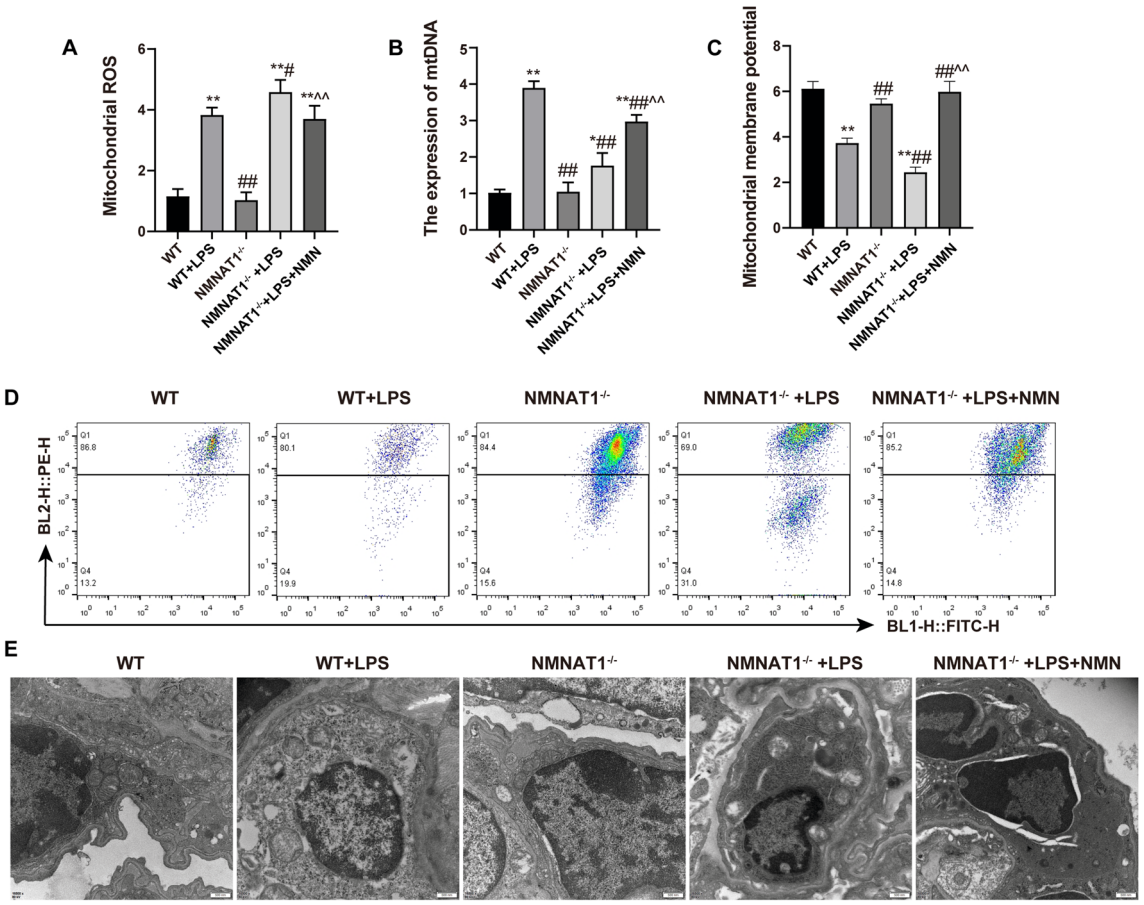

Fig. 3 NAD$^+$ protected against mitochondrial dysfunction. **A** Mitochondrial ROS detected spectrofluorometrically using DCFH-DA as a fluorescent dye. **B** Mitochondrial DNA copy number (mtDNA-CN) in each group was measured using RT-PCR. **C** The columnar picture is the statistical analysis of the mitochondrial membrane potential. **D** The mitochondrial membrane potential (ΔΨm) changes in lung tissue were evaluated using JC-1 fluorescence dye by flow cytometry. Q1, red fluorescence + /green fluorescence, polarized ΔΨm; Q4, red fluorescence + /green fluorescence, depolarized ΔΨm. **E** The morphological alterations of mitochondria by transmission electron microscopy (Scale bar: 500 nm). Data are presented as mean ± SD and group comparisons were analyzed by one-way ANOVA followed by Bonferroni post hoc test. $^{*}P<0.05$, $^{**}P<0.01$ versus WT group, $^{\#}P<0.05$, $^{\#\#}P<0.01$ versus WT + LPS group, and $^{\wedge}P<0.05$, $^{\wedge\wedge}P<0.01$ versus NMNAT1$^{-/-}$ + LPS group, respectively

severe mitochondria damage with swollen, fragmented, even absent cristae and lipofuscin deposits than WT mice (Fig. 3E). And, compared to the WT + LPS group, mitochondrial ROS in NMNAT1$^{-/-}$ + LPS group was significantly increased, while the mtDNA and ΔΨm were marked decreased, indicating that mitochondrial structural injury and the functional decline were more significant severe (Fig. 3A–D). However, the dysfunction and altered morphology of mitochondria were improved by NMN pretreatment (Fig. 3A–E). These results suggest that restoring NAD$^+$ levels is crucial for protecting from LPS-induced mitochondrial oxidative damage and maintaining the structural integrity of mitochondria.

NAD$^+$ levels maintained mitonuclear communication in sepsis-induced ALI

Mitonuclear protein imbalance and the mitochondrial unfolded protein response (UPR^{mt}) are two essential mechanisms that play pivotal roles in regulating mitonuclear communication, which seems to be an important adaptive response against oxidative stress [16, 41]. Given the key role of NAD$^+$ for cellular homeostasis and mitochondrial functions, we hypothesized that NAD$^+$ concentrations are responsible for mitonuclear protein imbalance and UPR^{mt} during sepsis-induced ALI. Thus, the expression of several markers critical in mitonuclear protein imbalance and UPR^{mt} was determined, including the ratio of succinate dehydrogenase A (SDHA) to cytochrome c oxidase subunit (MTCO1) symbolizing the balance between nDNA- and mtDNA-encoded oxidative phosphorylation (OXPHOS) subunit, and the expressions of UPR^{mt} biomarkers HSP60, LONP1, and HSP90 [13, 18, 42, 43].

Compared with the WT group, the SDHA/MTCO1 ratio and the expression of HSP60, LONP1, and HSP90 were increased when mice were subjected to LPS demonstrating a defensive action to oxidative stress (Fig. 4A–E). However, the ratio of SDHA/MTCO1 and UPR^{mt} biomarkers was decreased in NMNAT1$^{-/-}$ mice treated with LPS relative to WT mice (Fig. 4A–E). Furthermore, NMN induced a striking mitonuclear protein imbalance and UPR^{mt} as evidenced by induction of SDHA/MTCO1 ratio and HSP60, LONP1, and HSP90 expressions (Fig. 4A–E).

HO-1 protected against ALI via NAD$^+$-dependent manner

To determine whether the protective effect of HO-1 depends on NAD$^+$, we examined the effect of HO-1 on NMNAT1-deficient mice and equivalently damaged wild-type mice treated with LPS. As shown in Fig. 5, NAD$^+$ levels in the LPS plus hemin-treated NMNAT1$^{-/-}$ mice were distinctly reduced than that in WT mice (Fig. 5A). The histopathological changes, including thickened alveolar septa, aggravated neutrophil infiltration, and hemorrhage induced by LPS, were exacerbated in that hemin-treated NMNAT1$^{-/-}$ mice, also shown by the lung injury score intuitively (Fig. 5B and C). Further studies

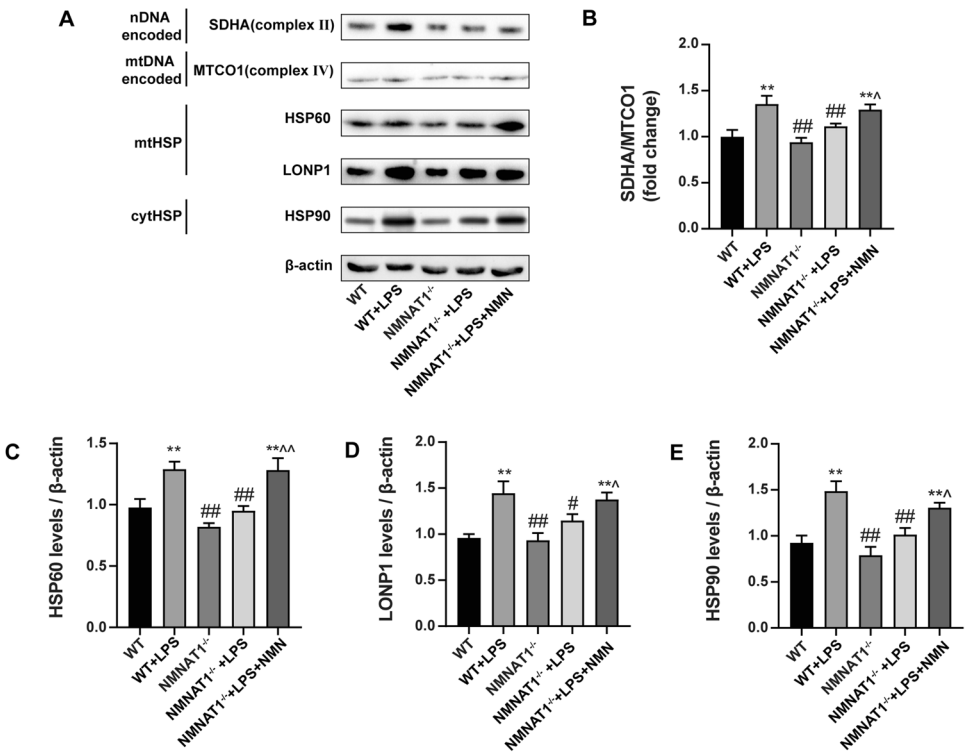

Fig. 4 NAD$^+$ levels preserved the mitonuclear communication. **A** Representative Western blot of mitonuclear protein imbalance (MTCO1 and SDHA) and UPR^{mt} (HSP60, LONP1, HSP90) markers. **B–E** Quantification of the ratio of SDHA/MTCO1 and expressions of HSP60, LONP1, HSP90. Band intensity on the Western blotting images was expressed as their relative ratio compared with β-actin. Data are presented as mean ± SD and statistical analysis was performed by one-way analysis of variance followed by Bonferroni post hoc test. $^{*}P<0.05$, $^{**}P<0.01$ versus WT group, $^{\#}P<0.05$, $^{\#\#}P<0.01$ versus WT + LPS group, and $^{\wedge}P<0.05$, $^{\wedge\wedge}P<0.01$ versus NMNAT1$^{-/-}$ + LPS group, respectively

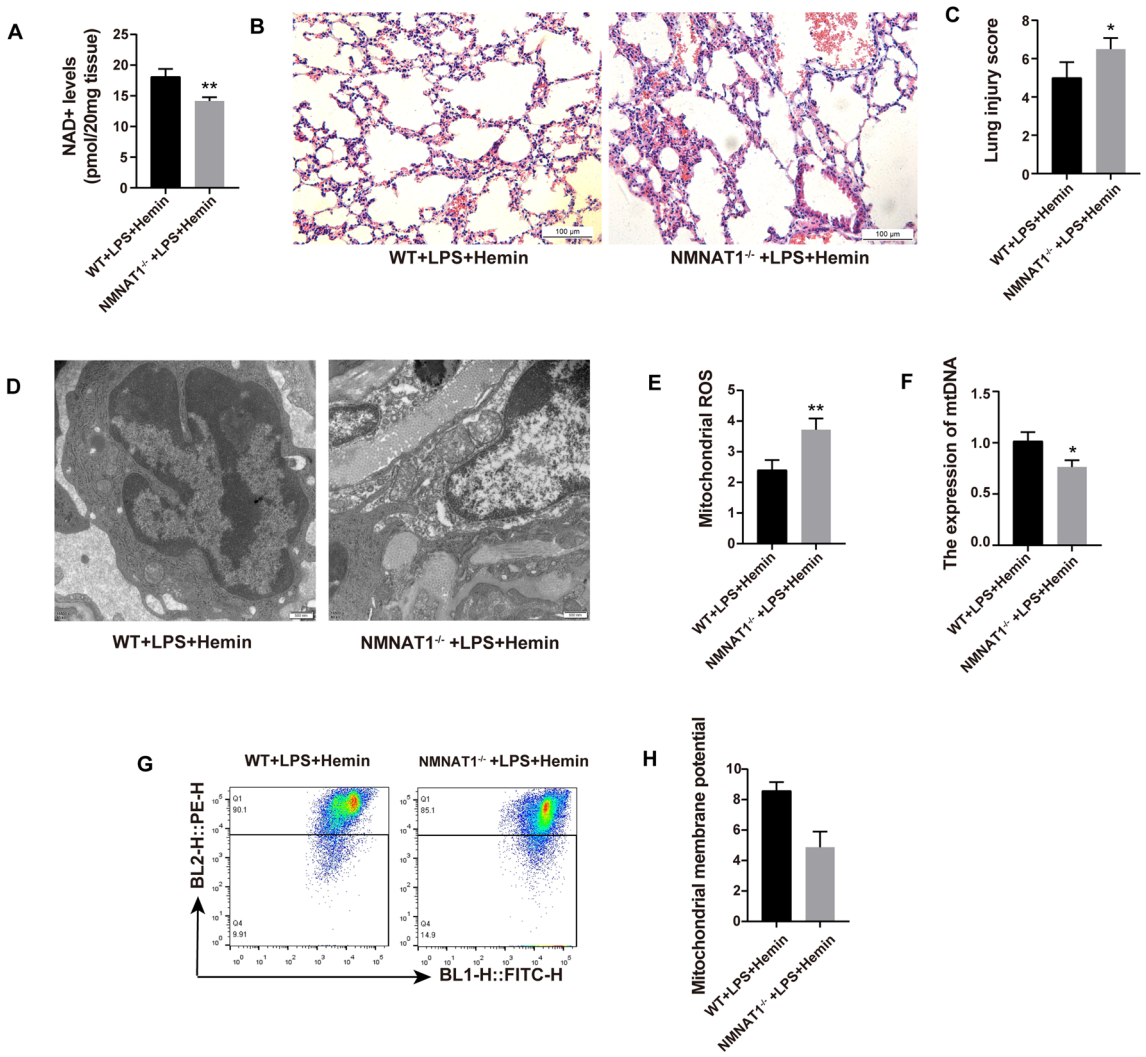

Fig. 5 The effect of HO-1 depended on NAD^+ levels. **A** NAD^+ contents in lung tissue. **B** Photomicrographs of histopathologic changes of lung sections stained with hematoxylin and eosin (×200). **C** Semi-quantitative analysis of lung tissues by lung injury scores. **D** The morphological alterations of mitochondria by transmission electron microscopy (Scale bar: 500 nm). **E** Mitochondrial ROS detected spectrofluorometrically using DCFH-DA as a fluorescent dye. **F** Mitochondrial DNA copy number (mtDNA-CN) in each group was measured using RT-PCR. **G** The mitochondrial membrane potential ($\Delta\Psi m$) changes in lung tissue were evaluated using JC-1 fluorescence dye by flow cytometry. **H** The columnar picture is the statistical analysis of the mitochondrial membrane potential. Results are presented as mean ± SD and statistical analysis was performed by paired *t*-test. $^{*}P<0.05$, $^{**}P<0.01$

on the morphology and function of mitochondria were performed; there were more abnormal characteristics of mitochondrial ultrastructure, including swollen mitochondria and fractured cristae in NMNAT1$^{-/-}$ + LPS + Hemin mice (Fig. 5D). Mitochondrial ROS contents were significantly increased for NMNAT1$^{-/-}$ mice, whereas mtDNA and mitochondrial membrane potential were reduced (Fig. 5E–H). The data supported that HO-1 rescued sepsis-induced ALI in an NAD^+-dependent manner.

Protective effect of HO-1 required NAD^+-mediated mitonuclear communication

Having shown the critical role of NAD^+ in mitonuclear protein imbalance and UPR^{mt} during sepsis-induced ALI, we hypothesized subsequently that HO-1 might require NAD^+-mediated mitonuclear communication to exert lung protection. As shown in Fig. 6, the SDHA/MTCO1 ratio and biomarkers of UPR^{mt}, including HSP60, LONP1, and

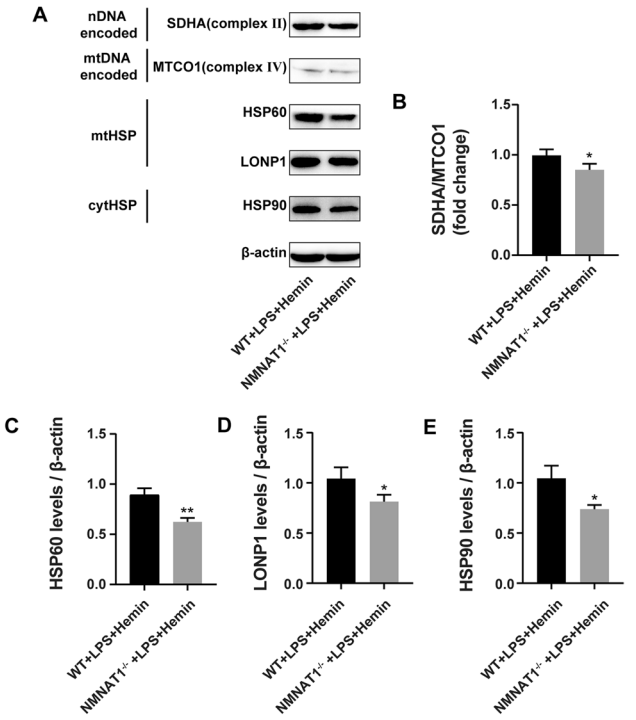

Fig. 6 The effect of HO-1 required NAD^+-mediated mitonuclear protein imbalance and UPR^{mt}. **A** The protein expression levels of SDHA, MTCO1, HSP60, LONP1, HSP90 in lung extracts were detected by Western blotting. Band intensity on the western blotting images was expressed as their relative ratio compared with β-actin. **B**–**E** Quantification from Western blotting to assess the expressions of proteins. All data are presented as mean ± SD, and statistical analysis was performed by paired *t*-test. $^{*}P<0.05$, $^{**}P<0.01$

HSP90, were decreased in hemin-treated NMNAT1$^{-/-}$ mice with ALI. Therefore, the beneficial effects of HO-1 on sepsis-induced ALI require NAD^+-mediated mitonuclear communication.

HO-1 mitigated LPS-induced ALI by preserving NAD^+-mediated mitonuclear communication through PGC1α/PPARγ signaling pathway

PGC1α is a critical regulatory gene of mitochondrial biogenesis that can be activated by NAD^+ and its dependent deacetylase, and acts as a transcription coactivator to enhance the activity of PPARγ [44, 45]. It has been found that the activation of the PGC1α/PPARγ axis is an effective intervention to prevent or restore oxidative stress-induced mitochondrial dysfunction and has proven to be a promising treatment strategy for sepsis [44, 46]. In order to figure out the relationship between PGC1α/PPARγ signaling pathway and HO-1/NAD^+-mediated mitonuclear communication, we examined the effect of SR-18292, a selective inhibitor of PGC1α on hemin-treated septic mice. As shown in Fig. 7A, NAD^+ level was decreased after SR-18292 administration. Histopathological analysis revealed aggravated lung injury in SR-18292-treated mice, characterized by interstitial edema, hemorrhage, and inflammatory infiltrate (Fig. 7B). And, this was concurrent with elevated lung injury scores in SR-18292-treated mice (Fig. 7C). At the same time, the alterations in morphology and biogenesis of mitochondria were observed in the experiment. As shown in Fig. 7D and E, pretreatment of mice with SR-18292 induced a decrease in mtDNA and marked structural abnormalities of mitochondria. Furthermore, mice exposed to SR-18292 showed a striking decrease in the SDHA/MTCO1 ratio and the expressions of HSP60, LONP1, and HSP90 (Fig. 7F, G). The results supported a critical role of the PGC1α/PPARγ signaling pathway on HO-1 afforded the NAD^+-mediated mitochondria communication.

Discussion

The present study showed that the HO-1 exerted lung-protective effect and the expressions of HO-1 affect the levels of NAD^+ during endotoxin-induced acute lung injury. The following experiment reveals the basis for potential applications of NAD^+ for treating acute lung injury and focuses NAD^+ on mitonuclear protein imbalance and UPR^{mt} for protection against LPS-induced ALI. Furthermore, the shortage of NAD^+ substantially blunted the protective effect of HO-1, which aggravated lung damage and mitochondrial dysfunction, and suppressed the mitonuclear protein imbalance and UPR^{mt}, indicating that the lung-protective effect of HO-1 depends on NAD^+ levels and requires NAD^+-mediated mitonuclear communication. And the inhibition of PGC1α/PPARγ signaling pathway was validated in HO-1 afforded the regulation of NAD^+-mediated mitonuclear communication.

Mitochondria are dynamic organelles and act as the center stage for energy metabolism, signal transduction, and stress response [47]. Mitochondrial dysfunction has long been implicated in sepsis, mainly as a source of oxidative stress and ROS [47]. A growing number of studies showed that the mitochondria-centered cellular network, the most crucial of which is the mitonuclear communication, requires them to regulate cellular needs and transcriptional programs, thereby alleviating mitochondrial dysfunction and maintaining cellular homeostasis [10]. Mitonuclear protein imbalance characterized by an altered balance between nDNA- and mtDNA-encoded OXPHOS subunits and UPR^{mt} are induced by mitochondrial stress, subsequently surging a nuclear transcriptional response, including the chaperones HSP60, LONP1, and HSP90, to restore mitochondrial proteostasis [16, 17]. Thus, both mitonuclear protein imbalance and UPR^{mt} are important mechanisms for mitonuclear communication [11, 14]. While mounting evidence shows the

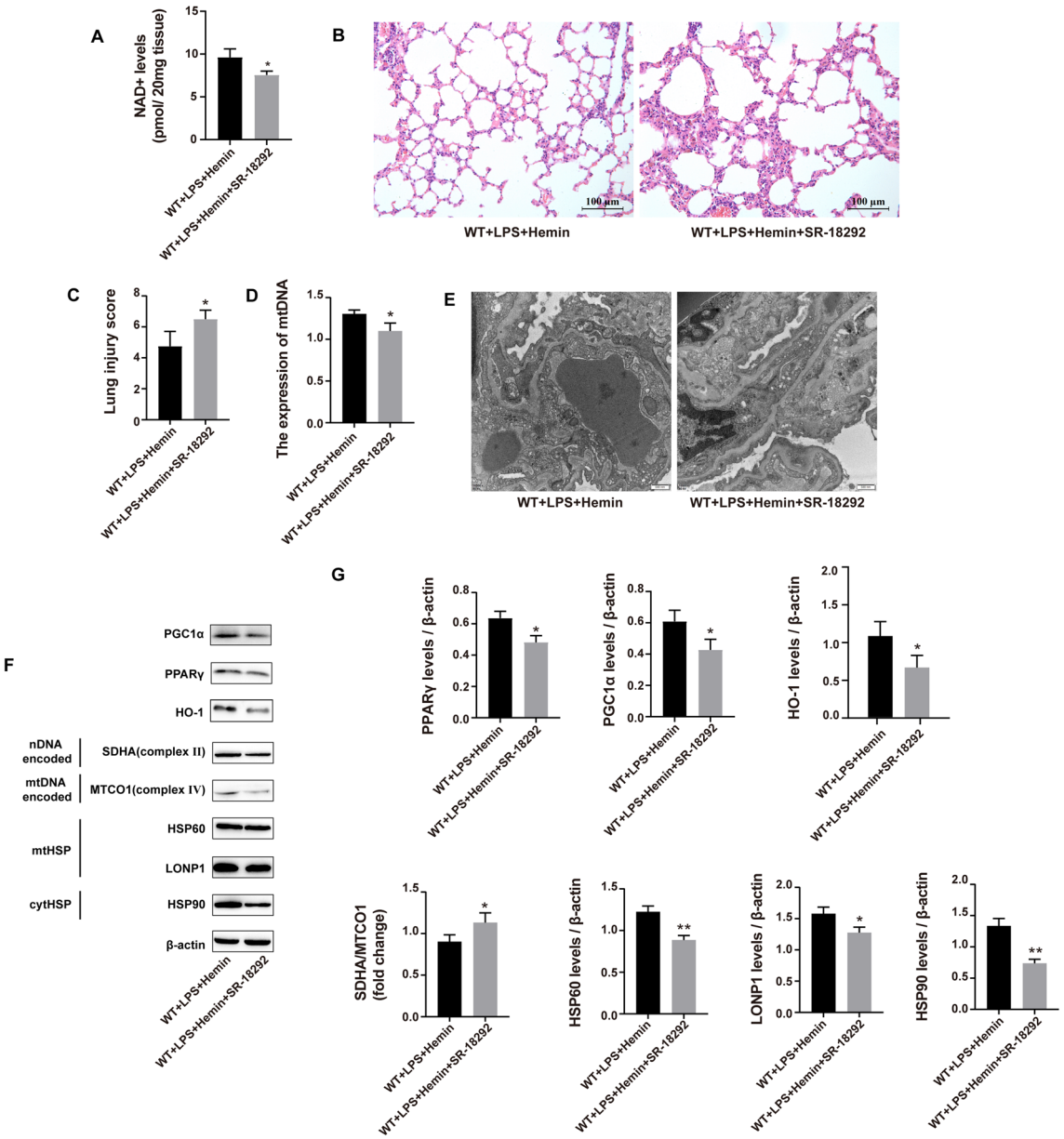

Fig. 7 PGC1α/PPARγ axis involved the regulation of HO-1/NAD^+-mediated mitonuclear communication. **A** NAD^+ levels. **B** Pathological changes of lung sections stained with H&E were observed by light microscopy (×200). **C** Semiquantitative analysis of lung tissues by lung injury scores. **D** RT-PCR was used to measure the mitochondrial DNA (mtDNA) levels in the lung extracts. **E** Transmission electron microscopy (TEM) was utilized to investigate the ultrastructural changes of the mitochondria. (Scale bar: 500 nm). **F**, **G** The relative expression of PGC1α, PPARγ, HO-1, mito-encoded MTCO1 and nc-encoded SDHA, UPR^{mt}-related proteins HSP60, LONP1, and HSP90. Data are represented as mean ± SD and were analyzed by paired *t*-test. $^{*}P<0.05$, $^{**}P<0.01$

importance of adaptive mechanisms to age-related metabolism but few in inflammatory diseases [16, 41].

Our previous studies have proved that HO-1 exhibits extensive protection both in LPS-stimulated RAW 264.7 cells and in a murine model of LPS-induced ALI by preserving mitochondrial dynamics through regulating fission and fusion [7, 23, 24]. Given the critical role of HO-1 on mitochondrial function and oxidative stress, we hypothesized that the protective effect of HO-1 might be associated with mitonuclear communication. Widely literature search revealed intimate links between HO-1 and NAD^+, which exerts a predominant role in sensing and communicating between mitochondria and the nucleus [10, 41]. The second step of heme degradation generates additional NAD^+, which also influences glycometabolism, including the pentose phosphate pathway and TCA cycle [33]. On the other

hand, HO-1-derived CO targets mitochondrial respiration and glycometabolism, which are closely associated with NAD^+ to prevent pathological damage [33]. Together, these studies provide a clue between HO-1 and NAD^+ during sepsis-induced ALI. In the current study, a significant increase in NAD^+ levels along with upregulation of HO-1 was observed in septic mice with hemin pretreatment, while a district reduction of NAD^+ in HO-1 knockout mice, indicating that the protective effect of HO-1 might be related to NAD^+ levels. Furtherly, we found that the knockout in the critical enzyme of NAD^+ biosynthesis NMNAT1 weakened the protective effect of HO-1 against oxidative stress and lung damage and caused mitonuclear protein imbalance and UPR^{mt} partially loss. Collectively, these data suggested that the protective effect of HO-1 depends on NAD^+ levels and requires NAD^+-mediated mitonuclear communication.

NAD^+, a widely present coenzyme, is an important regulator of cellular metabolism and homeostasis. There are three major pathways contributing to NAD^+ synthesis in which the salvage pathway accounts for most of the NAD^+ in mammals [48, 49]. Briefly, NAD^+ is converted from NMN by NMNATs, and NMNAT1 is ubiquitously expressed with the highest affinity for substrates and highest enzyme activity [48]. In addition to energy metabolism, NAD^+ homeostasis provides a link between pro-inflammatory response and redox status [28, 50]. A lung-protective effect of NAD^+ has been detected with LPS-induced ALI in mice, although the mechanism remains unclear [30, 50, 51]. Thus, the deficit of NMNAT1 and administration of NMN were designed to alter cellular NAD^+ levels to explore its action in sepsis-induced ALI. Interestingly, impairment of NAD^+ biosynthesis caused by NMNAT1 deficiency exhibited a strange scene: slender alveolar septa, malnourished, but without obviously mitochondrial dysfunction and structural damage. However, $NMNAT1^{-/-}$ mice surged more severe inflammatory responses and mitochondrial dysfunction when attacked by LPS, which might be explained by the straight decline of NAD^+ levels impaired the ability of resistance. And restoring NAD^+ by supplementation of NMN improves mitochondrial disorders and mitigates lung injury. Further study showed significant decreases of SDHA/MTCO1 ratio and the expression of HSP60, LONP1 and HSP90 in $NMNAT1^{-/-}$ mice subjected to LPS, while replenished NAD^+ levels upregulated the mitochondrial proteostasis and UPR^{mt}, suggesting that the protective effect of NAD^+ is associated with mitonuclear imbalance.

PGC1α/PPARγ signaling pathway represented a pivotal cytoprotective mechanism against diverse pathophysiological processes, such as acute inflammatory diseases, diabetes, and aging [52]. PGC1α/PPARγ axis has been reported to be a target of HO-1 and the deacetylation of PGC1α is regulated by NAD^+ and NAD^+-dependent deacetylase SIRT1 [44, 53, 54]. To define the relationship between PGC1α/PPARγ pathway and HO-1/NAD^+-mediated mitonuclear communication during sepsis-induced ALI, SR-18292, a selective PGC1α inhibitor, was treated with mice exposed to LPS and hemin. As expected, the inhibition of PGC1α/PPARγ aggravated the pathological damage and mitochondrial dysfunction and decreased the SDHA/MTCO1 ratio and the expression of HSP60, LONP1, and HSP90.

The limitations of the present study are worth noting. Mitonuclear communication is a highly complex process that requires precise regulation and crosstalk. The present study aimed at adaptive response, including mitonuclear protein imbalance and UPR^{mt} to elaborate mitonuclear imbalance, but the specific regulatory mediator or bridge directly deserves to be explored intensively. In addition, sirtuins, the NAD^+-dependent protein deacetylases, are recognized as potential therapeutic targets for regulating the acute inflammatory response. Thus, whether sirtuins participate in the protective mechanism of HO-1 against sepsis-induced ALI needs to be explored in the future.

Conclusions

In summary, HO-1 protects against septic lung injury by regulating NAD^+ levels and preserving NAD^+-mediated mitonuclear communication, modulating the mitonuclear protein imbalance and UPR^{mt} markers through the PGC1α/PPARγ signaling pathway. NAD^+ levels are susceptible to endotoxin-induced ALI and influence lung damage inversely, and its protective role might be associated with mitonuclear communication. The study provides novel insights into the protective effects of HO-1, which depends on NAD^+ levels and NAD^+-mediated mitonuclear communication, which might represent rationales for treating sepsis-related ALI.

Acknowledgements This work was supported by the National Natural Science Foundation of China (82004076 and 81772106) and the Natural Science Foundation of Tianjin (20JCYBJC00540, 20JCZDJC00480). And the authors wish to acknowledge Tianjin key Laboratory of Acute Abdomen Disease Associated Organ Injury and ITCWM Repair, Institute of Acute Abdominal Diseases for providing a reliable platform for scientific research.

Author contributions J.B.Y and J.S. conceived, designed, and supervised the experiments; J.B.Y, J.S., and S.A.D., and L.R.G. secured funding to support this project and overall study; S.M.H. performed the experiments, interpreted results, and wrote the manuscript; J.Y. and Q.Y.G. performed the experiments and provided technical supports; W.M.L. corrected the manuscript; S.H.D. assisted with statistical analysis; Y.Z. and X.Y.L. interpreted the results and consulted related references. All authors reviewed the manuscript.

Declarations

Conflict of interest No conflicts of interest are declared by the authors.

References

1. van der Poll T, et al. The immunopathology of sepsis and potential therapeutic targets. Nat Rev Immunol. 2017;17:407–20. https://doi.org/10.1038/nri.2017.36.
2. Fowler AA 3rd, et al. Effect of vitamin C infusion on organ failure and biomarkers of inflammation and vascular injury in patients with sepsis and severe acute respiratory failure: the CITRIS-ALI randomized clinical trial. JAMA. 2019;322:1261–70. https://doi.org/10.1001/jama.2019.11825.
3. Bellani G, et al. Epidemiology, patterns of care, and mortality for patients with acute respiratory distress syndrome in intensive care units in 50 countries. JAMA. 2016;315:788–800. https://doi.org/10.1001/jama.2016.0291.
4. Cao X. COVID-19: immunopathology and its implications for therapy. Nat Rev Immunol. 2020;20:269–70. https://doi.org/10.1038/s41577-020-0308-3.
5. Huang C, et al. Clinical features of patients infected with 2019 novel coronavirus in Wuhan, China. The Lancet. 2020;395:497–506. https://doi.org/10.1016/s0140-6736(20)30183-5.
6. Arulkumaran N, et al. Mitochondrial function in sepsis. Shock. 2016;45:271–81. https://doi.org/10.1097/shk.0000000000000463.
7. Yu J, et al. Heme oxygenase-1/carbon monoxide-regulated mitochondrial dynamic equilibrium contributes to the attenuation of endotoxin-induced acute lung injury in rats and in lipopolysaccharide-activated macrophages. Anesthesiology. 2016;125:1190–201. https://doi.org/10.1097/aln.0000000000001333.
8. Fredriksson K, et al. Mitochondrial function in sepsis: respiratory versus leg muscle. Crit Care Med. 2007;35:S449-453. https://doi.org/10.1097/01.Ccm.0000278048.00896.4b.
9. D'Amico D, et al. Cytosolic proteostasis networks of the mitochondrial stress response. Trends Biochem Sci. 2017;42:712–25. https://doi.org/10.1016/j.tibs.2017.05.002.
10. Mottis A, et al. Mitocellular communication: Shaping health and disease. Science (New York, NY). 2019;366:827–32. https://doi.org/10.1126/science.aax3768.
11. Quirós PM, et al. Mitonuclear communication in homeostasis and stress. Nat Rev Mol Cell Biol. 2016;17:213–26. https://doi.org/10.1038/nrm.2016.23.
12. Pellegrino MW, et al. Mitochondrial UPR-regulated innate immunity provides resistance to pathogen infection. Nature. 2014;516:414–7. https://doi.org/10.1038/nature13818.
13. Xu M, et al. Choline ameliorates cardiac hypertrophy by regulating metabolic remodelling and UPRmt through SIRT3-AMPK pathway. Cardiovasc Res. 2019;115:530–45. https://doi.org/10.1093/cvr/cvy217.
14. Zhou H, et al. Loss of high-temperature requirement protein A2 protease activity induces mitonuclear imbalance via differential regulation of mitochondrial biogenesis in sarcopenia. IUBMB Life. 2020;72:1659–79. https://doi.org/10.1002/iub.2289.
15. Melber A, et al. UPR(mt) regulation and output: a stress response mediated by mitochondrial-nuclear communication. Cell Res. 2018;28:281–95. https://doi.org/10.1038/cr.2018.16.
16. Houtkooper RH, et al. Mitonuclear protein imbalance as a conserved longevity mechanism. Nature. 2013;497:451–7. https://doi.org/10.1038/nature12188.
17. Haynes CM, et al. The mitochondrial UPR—protecting organelle protein homeostasis. J Cell Sci. 2010;123:3849–55. https://doi.org/10.1242/jcs.075119.
18. Moullan N, et al. Tetracyclines disturb mitochondrial function across eukaryotic models: a call for caution in biomedical research. Cell Rep. 2015;10:1681–91. https://doi.org/10.1016/j.celrep.2015.02.034.
19. English J, et al. Decoding the rosetta stone of mitonuclear communication. Pharmacol Res. 2020;161: 105161. https://doi.org/10.1016/j.phrs.2020.105161.
20. Lv H, et al. Isovitexin exerts anti-inflammatory and anti-oxidant activities on lipopolysaccharide-induced acute lung injury by inhibiting MAPK and NF-κB and activating HO-1/Nrf2 pathways. Int J Biol Sci. 2016;12:72–86. https://doi.org/10.7150/ijbs.13188.
21. Shi J, et al. PI3K/Akt pathway-mediated HO-1 induction regulates mitochondrial quality control and attenuates endotoxin-induced acute lung injury. Lab Invest. 2019;99:1795–809. https://doi.org/10.1038/s41374-019-0286-x.
22. Zhang L, et al. Isoflavone ME-344 disrupts redox homeostasis and mitochondrial function by targeting heme oxygenase 1. Cancer Res. 2019;79:4072–85. https://doi.org/10.1158/0008-5472.Can-18-3503.
23. Shi J, et al. Dexmedetomidine ameliorates endotoxin-induced acute lung injury in vivo and in vitro by preserving mitochondrial dynamic equilibrium through the HIF-1a/HO-1 signaling pathway. Redox Biol. 2021;41: 101954. https://doi.org/10.1016/j.redox.2021.101954.
24. Shi J, et al. Hydromorphone protects against CO(2) pneumoperitoneum-induced lung injury via heme oxygenase-1-regulated mitochondrial dynamics. Oxid Med Cell Longev. 2021;2021:9034376. https://doi.org/10.1155/2021/9034376.
25. Li X, et al. Heme oxygenase-1(HO-1) regulates Golgi stress and attenuates endotoxin-induced acute lung injury through hypoxia inducible factor-1α (HIF-1α)/HO-1 signaling pathway. Free Radical Biol Med. 2021;165:243–53. https://doi.org/10.1016/j.freeradbiomed.2021.01.028.
26. Bi XG, et al. Helix B surface peptide protects against acute lung injury through reducing oxidative stress and endoplasmic reticulum stress via activation of Nrf2/HO-1 signaling pathway. Eur Rev Med Pharmacol Sci. 2020;24:6919–30. https://doi.org/10.26355/eurrev_202006_21683.
27. Nikiforov A, et al. The human NAD metabolome: functions, metabolism and compartmentalization. Crit Rev Biochem Mol Biol. 2015;50:284–97. https://doi.org/10.3109/10409238.2015.1028612.
28. Zhang DX, et al. The potential regulatory roles of NAD(+) and its metabolism in autophagy. Metabolism. 2016;65:454–62. https://doi.org/10.1016/j.metabol.2015.11.010.
29. Cambronne XA, et al. Biosensor reveals multiple sources for mitochondrial NAD^+. Science (New York, NY). 2016;352:1474–7. https://doi.org/10.1126/science.aad5168.
30. Hong G, et al. Administration of nicotinamide riboside prevents oxidative stress and organ injury in sepsis. Free Radical Biol Med. 2018;123:125–37. https://doi.org/10.1016/j.freeradbiomed.2018.05.073.
31. Tran MT, et al. PGC1α drives NAD biosynthesis linking oxidative metabolism to renal protection. Nature. 2016;531:528–32. https://doi.org/10.1038/nature17184.
32. Lee CF, et al. Normalization of NAD+ redox balance as a therapy for heart failure. Circulation. 2016;134:883–94. https://doi.org/10.1161/circulationaha.116.022495.
33. Wegiel B, et al. Heme oxygenase-1: a metabolic nike. Antioxid Redox Signal. 2014;20:1709–22. https://doi.org/10.1089/ars.2013.5667.

34. Vettorazzi S, et al. Glucocorticoids limit acute lung inflammation in concert with inflammatory stimuli by induction of SphK1. Nat Commun. 2015;6:7796. https://doi.org/10.1038/ncomms8796.
35. Ye Z, et al. LncRNA-LET inhibits cell growth of clear cell renal cell carcinoma by regulating miR-373-3p. Cancer Cell Int. 2019;19:311. https://doi.org/10.1186/s12935-019-1008-6.
36. Le Ribeuz H, et al. Proteomic analysis of KCNK3 loss of expression identified dysregulated pathways in pulmonary vascular cells. Int J Mol Sci. 2020. https://doi.org/10.3390/ijms21197400.
37. Imai SI, et al. It takes two to tango: NAD(+) and sirtuins in aging/longevity control. NPJ Aging Mech Dis. 2016;2:16017. https://doi.org/10.1038/npjamd.2016.17.
38. Cantó C, et al. NAD(+) metabolism and the control of energy homeostasis: a balancing act between mitochondria and the nucleus. Cell Metab. 2015;22:31–53. https://doi.org/10.1016/j.cmet.2015.05.023.
39. Zapata-Pérez R, et al. Reduced nicotinamide mononucleotide is a new and potent NAD(+) precursor in mammalian cells and mice. FASEB J. 2021;35: e21456. https://doi.org/10.1096/fj.202001826R.
40. Wu Y, et al. Mitochondrial quality control mechanisms as potential therapeutic targets in sepsis-induced multiple organ failure. J Mol Med (Berl). 2019;97:451–62. https://doi.org/10.1007/s00109-019-01756-2.
41. Karpac J, et al. Aging: seeking mitonuclear balance. Cell. 2013;154:271–3. https://doi.org/10.1016/j.cell.2013.06.046.
42. Chen J, et al. Oxidative stress induces different tissue dependent effects on Mutyh-deficient mice. Free Radical Biol Med. 2019;143:482–93. https://doi.org/10.1016/j.freeradbiomed.2019.09.005.
43. Cordeiro AV, et al. Aerobic exercise training induces the mitonuclear imbalance and UPRmt in the skeletal muscle of aged mice. J Gerontol. 2020;75:2258–61. https://doi.org/10.1093/gerona/glaa059.
44. Wang W, et al. MAR1 suppresses inflammatory response in LPS-induced RAW 264.7 macrophages and human primary peripheral blood mononuclear cells via the SIRT1/PGC-1α/PPAR-γ pathway. J Inflamm (London, England). 2021;18:8. https://doi.org/10.1186/s12950-021-00271-x.
45. Zhang T, et al. Overexpression of peroxisome proliferator-activated receptor γ coactivator 1-α protects cardiomyocytes from lipopolysaccharide-induced mitochondrial damage and apoptosis. Inflammation. 2020;43:1806–20. https://doi.org/10.1007/s10753-020-01255-4.
46. Peng S, et al. PPAR-γ activation prevents septic cardiac dysfunction via inhibition of apoptosis and necroptosis. Oxid Med Cell Longev. 2017;2017:8326749. https://doi.org/10.1155/2017/8326749.
47. Balaban RS, et al. Mitochondria, oxidants, and aging. Cell. 2005;120:483–95. https://doi.org/10.1016/j.cell.2005.02.001.
48. Yang T, et al. NAD metabolism and sirtuins: metabolic regulation of protein deacetylation in stress and toxicity. AAPS J. 2006;8:E632-643. https://doi.org/10.1208/aapsj080472.
49. Massudi H, et al. NAD+ metabolism and oxidative stress: the golden nucleotide on a crown of thorns. Redox Rep. 2012;17:28–46. https://doi.org/10.1179/1351000212y.0000000001.
50. Al-Shabany AJ, et al. Intracellular NAD+ levels are associated with LPS-induced TNF-α release in pro-inflammatory macrophages. Biosci Rep. 2016;36: e00301. https://doi.org/10.1042/bsr20150247.
51. Liu TF, et al. NAD+-dependent SIRT1 deacetylase participates in epigenetic reprogramming during endotoxin tolerance. J Biol Chem. 2011;286:9856–64. https://doi.org/10.1074/jbc.M110.196790.
52. Fontecha-Barriuso M, et al. The role of PGC-1α and mitochondrial biogenesis in kidney diseases. Biomolecules. 2020. https://doi.org/10.3390/biom10020347.
53. Gomes AP, et al. Declining NAD(+) induces a pseudohypoxic state disrupting nuclear-mitochondrial communication during aging. Cell. 2013;155:1624–38. https://doi.org/10.1016/j.cell.2013.11.037.
54. Cho RL, et al. Heme oxygenase-1 induction by rosiglitazone via PKCα/AMPKα/p38 MAPKα/SIRT1/PPARγ pathway suppresses lipopolysaccharide-mediated pulmonary inflammation. Biochem Pharmacol. 2018;148:222–37. https://doi.org/10.1016/j.bcp.2017.12.024.